06 Apr 2023

Dynamic and Equilibrium Contribution of Nematic Order in Wetting and Contact Angles

Partho Neogi
Missouri University of Science and Technology, neogi@mst.edu

Xianjie Qiu

Amer Al-Shareef

Recommended Citation

P. Neogi et al., "Dynamic and Equilibrium Contribution of Nematic Order in Wetting and Contact Angles," *Journal of Physical Chemistry B*, vol. 127, no. 13, pp. 3071 - 3078, American Chemical Society, Apr 2023. The definitive version is available at https://doi.org/10.1021/acs.jpcb.2c08552

THE JOURNAL OF PHYSICAL CHEMISTRY B
A JOURNAL OF THE AMERICAN CHEMICAL SOCIETY

pubs.acs.org/JPCB

Article

Dynamic and Equilibrium Contribution of Nematic Order in Wetting and Contact Angles

P. Neogi,* Xianjie Qiu, and Amer Al-Shareef

Cite This: J. Phys. Chem. B 2023, 127, 3071−3078

Read Online

ACCESS | Metrics & More | Article Recommendations | Supporting Information

ABSTRACT: A model for the dynamic contact angles and the spreading kinetics of nematic liquid crystals on a solid surface is presented for the first time using the continuum theory of liquid crystals. The equations of motion for this system are integrated for a wedge or a drop that is thin and moves slowly. The dynamic contact angle is found to depend on the capillary number that represents the importance of viscocapillarity and on the elasticity number that is the ratio between the elastic and surface forces. The model provides an explanation for the extra volume dependence that is reported in experiments, as well as one case of recoil, and for the observation that very small drops were reported to be immobile. For the first time, these previous experimental observations are shown to be due to elastic effects.

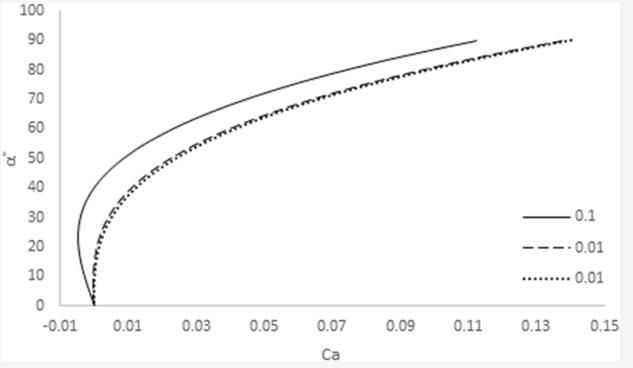

I. INTRODUCTION

When a drop is placed on the horizontal surface of a solid, it spreads outward. The rate at which it spreads is related to the angle that the drop makes with the solid surface, called the dynamic contact angle. Both the angle and the amount spread change with time, together, are referred to as spreading or wetting kinetics. This case is that of spontaneous spreading. There also is forced spreading, where a plate is plunged into a liquid. The main difference between the two is that the rate of spreading in forced spreading is an independent variable that covers a much larger range than in spontaneous spreading.[1] For nematic liquid crystals, some experimental data on spreading exist that do not conform with those for Newtonian liquids, as discussed below. Work on the fluid mechanics of nematic liquid crystals exists over a wide range, including cases that are somewhat similar to the system under consideration. Rey et al.[2,3] report that a variety of thin-film behavior under shear can give rise to oscillations in orientation. However, rotation will not occur in liquid crystals that have no cholesteric liquid crystals as in the work below. Many of the above studies also deal with polymeric liquid crystals, which have not been considered here. That is, the present system is a simple one where we show later both a correspondence with basic observations, as well as provide explanations for some striking features observed. Lin et al.[4] have provided a nonlinear stability analysis of dynamic contact lines—the result of which gives us important information that is used, as discussed later. We first consider the known features of isotropic liquids and then liquid crystals to be able to subtract off and retain the parts that are actually due to the special properties of liquid crystals, namely, elasticity and anisotropy. Knowledge of wetting kinetics of the kind investigated here is of importance in making liquid crystal displays where the liquid crystals are forced through two parallel plates.[5] Spontaneous spreading occurs when drops are layered to magnify fluorescence at molecular scales[6] on a solid surface.

A small liquid drop deposited on a solid surface can be wetting or nonwetting. A nonwetting drop at equilibrium has an equilibrium contact angle, λ, given by the Young−Dupré equation[1]

$$\gamma_{LV} \cos \lambda = \gamma_{SL} - \gamma_{SV} \quad (1)$$

where γ is the surface tension and S, L, and V are the solid, liquid, and vapor (air), respectively. While the equilibrium contact angle, λ, is routinely measured, surface tensions of solids are practically never measurable. Under nonequilibrium conditions, the drop shows a dynamic contact angle, α, and spreads out until the equilibrium configuration is reached,[1] Figure 1a. For a wetting liquid, $\lambda = 0°$, and the drop keeps spreading out. Instead of spontaneous spreading shown for the drop in Figure 1a, one can, instead, have a case of forced spreading, shown in Figure 1b when a plate is plunged into a liquid. Both cases describe advancing dynamic contact angles as shown. By retracting the plate, one can, instead, obtain a

Received: December 6, 2022
Revised: March 14, 2023
Published: March 28, 2023

https://doi.org/10.1021/acs.jpcb.2c08552
J. Phys. Chem. B 2023, 127, 3071−3078

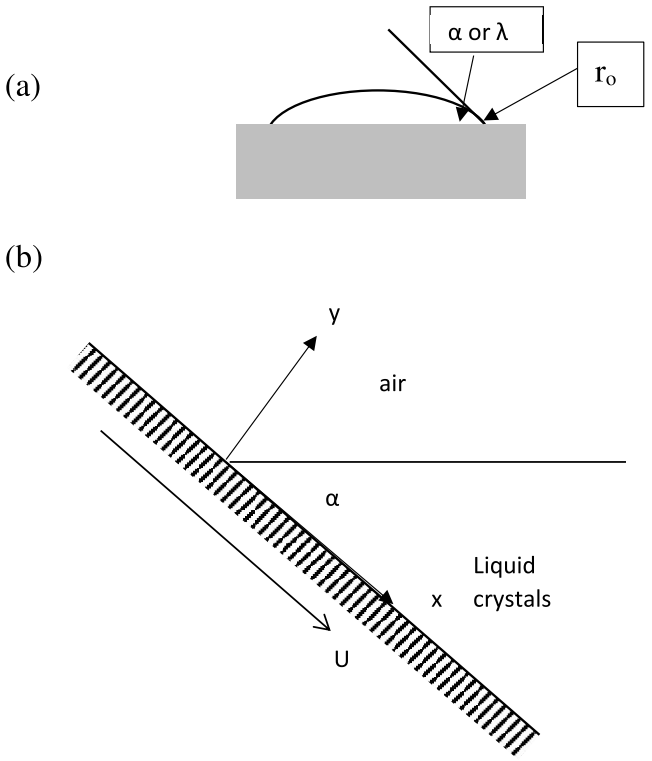

Figure 1. Basic geometry of the dynamic contact line (a) in a drop under spontaneous spreading and (b) the coordinate system is shown for forced spreading. The director **n** lies on the plane and is described by an angle θ between the director and the x-direction. Anchoring at the liquid−air interface makes the director perpendicular to the interface but along the solid surface. At the contact line, the film thickness is zero, and farther along in the x-direction, the film thickness is εL, which is the cutoff.

case of a receding dynamic contact angle where the substrate velocity U is in the direction opposite to the direction shown in Figure 1b.

I.I. Isotropic Liquids. Continuing the discussion of isotropic liquids, considerable attention has been paid to relating the wetting kinetics of drops, given by $\frac{dr_o}{dt}(=U)$, to α, where r_o is the basal radius of the drop, such as[7] $\frac{dr_o}{dt} \propto \alpha^2(\alpha - \gamma)$. For forced spreading, at sufficiently high values of U, the air is entrained into the liquid in Figure 1b and, in the receding case where U is in the other direction, the liquid is entrained. Although a quantitative description is available,[7,8] some features, such as the onset of air entrainment, have not yet been determined. In the model below, it is being assumed that the actual contact angle is λ but changes very quickly near the contact line to a slope of α based on the observation of Bascom et al.[9] These changes are at distances too small to be seen under microphotography.

Observations show that the dynamic contact line is at times unstable. The edge is seen to be scalloped.[10] Neogi[11] showed, theoretically, that the region of high curvature connecting the drop profiles with slopes of α and λ (for $\lambda = 0°$) was unstable and gave rise to a scalloped contact line. He could demonstrate a match between the predicted fastest-growing wavelength and that seen in the experiments by Williams.[10] In addition to the waves along the periphery, he also found that oscillations could occur perpendicular to the contact line.

I.II. Nematic Liquid Crystals. Starting with equilibrium, Cousins et al.[12] contend that the equilibrium contact angles in nematic liquid crystals can have more than one value for a droplet lying on a solid substrate, giving rise to a ridge. It would also lead to a non-circular contact line. Neither of these is observed in experiments on small drops[13−15] in many cases. However, a second equilibrium contact angle is predicted for the nematic liquid crystals below.

Lin et al.[15] measured the wetting kinetics of small drops of MBBA and EBBA on the surface of freshly cleaved mica under nitrogen. MBBA has equilibrium contact angles ($\lambda = 14°$ at 23 °C), which are small and appear to be independent of temperature. There is a nematic to isotropic transition temperature at 40 °C, and even above that, the liquid drop showed a small equilibrium contact angle at 45 °C. It was possible to measure the wetting kinetics of MBBA at 23 °C. It can be shown, using the available rate expressions, that there is a dependent dimensionless variable $r_o/V^{1/3}$ where V is the constant drop volume, and the capillary number is $Ca = \mu\frac{dr_o}{dt}/\gamma$ where μ is a nominal viscosity and γ is the surface tension. For constant μ and γ, instead of using the capillary number, one may plot $r_o/V^{1/3}$ vs $t/V^{1/3}$ (for $1/U$) to get plots independent of V. The spreading of drops of MBBA showed an extra dependence on V. EBBA showed small and temperature-dependent equilibrium contact angles, which appeared to go to zero at 60 °C. The dynamic contact angles obtained at 60 °C also showed the extra V dependence. The nematic to isotropic phase transition temperature for EBBA is at 80 °C.

The key feature in nematic liquid crystals is the nematic order given locally by the director vector **n**, which is the average molecular orientation there.[16] The elastic energy that restores the order is given by Oseen−Zöcher−Frank equation[16,17] as

$$\Phi = \frac{1}{2}k_{11}(\nabla\cdot\mathbf{n})^2 + \frac{1}{2}k_{22}(\mathbf{n}\cdot\nabla\times\mathbf{n})^2 + \frac{1}{2}k_{33}(\mathbf{n}\times\nabla\times\mathbf{n})^2 \quad (2)$$

From left to right, the terms correspond to the free energy change under molecular forces of orientation (i) when two neighboring molecules are separated on a curved surface, called splay, (ii) or twisted or twist, or (iii) on a surface that is bent, or bend. These can be given a complete molecular description using a molecular model.[17] They are shown schematically in the Supporting Information. k_{22} is zero for molecules that are not cholesteric, and it is assumed that the nematic liquid crystals under analysis are not cholesteric.

Anchoring at a boundary is a feature that distinguishes liquid crystals. It determines an angle at the interface shown in two dimensions in the Appendix as well. There is a particular direction at the surface according to energetic preference, with fluctuations as usual. If this energy is strong, then a fixed angle is obtained. This limit is that of strong anchoring used below. If the anchoring angle on one surface (liquid−vapor) is different from that on the other (liquid−solid), then the elastic forces in nematic liquid give rise to an excess potential, which is inversely proportional to h, the local film thickness.[13] Perez et al.[19] suggested that this potential energy be included in the disjoining pressure in a thin film. Neogi and Zhang[20] included this energy in calculating λ and h_o, the thickness of the thin film in equilibrium with the wedge, using the method of

https://doi.org/10.1021/acs.jpcb.2c08552
J. Phys. Chem. B 2023, 127, 3071−3078

Derjaguin and Frumkin.[21] Reasonable estimates for a number of parameters were used to calculate the two quantities above, which provided reasonable values for λ and h_o. It should be mentioned that although Rey and Tusuji[2] have reported a variety of flow behavior with changes in anchoring in their computations, Shmeliova et al.[22] do not see much change in their experimental work. It is possible that the flow in the liquid film has to be thin for the anchoring to have an effect, as seen near the contact line. Rough surfaces can induce nematic-isotropic phase transitions at the surface;[23] however, the experiments on surfaces considered below should have very low roughnesses. Brown et al.[24] observe that in an electric field, the equilibrium contact angle of a nematic liquid crystal changes by an amount that is the same for an isotropic liquid, even though the liquid crystals have an anisotropic permittivity. Mena et al.[25] have calculated the nature of flow in an electric field. Wei and Li[26] have considered the effect of polymer conformation near the contact line on contact angles and drop shapes. In principle, these concepts could be extended to polymeric liquid crystals. However, polymeric liquid crystals are not considered here as their rheology is complex.[3]

According to de Gennes and Prost,[18] the region immediately above the nematic to isotropic transition temperature shows slow relaxation and may help to explain why MBBA shows the same kind of wetting kinetics at 45 °C as it does below the transition temperature of 40 °C. In one case, EBBA showed a recoil, that is, the drop spread out and then retracted. Later experimental work by Poulard and Cazabat[13] with 5CB on oxidized silicon wafers also showed the above extra volume dependence. In addition, some drops did not move. They also observed instability in the form of a scalloped contact line. Forced spreading on a flat plate was reported much earlier by Jérôme and Biox[27] for a commercial mix of liquid crystals on an SiO surface. They discovered oscillations perpendicular to the contact line over a range of intermediate velocities, which were explained by them to be caused by bistable anchoring.

It is seen that both kinds of instabilities predicted for isotropic liquids[11] are actually observed in nematic liquid crystals: a scalloped contact line and oscillations perpendicular to the contact line. Pollard and Cazabat[13] observed unstable contact lines that are not just wavy, but some mushrooming of the protrusions takes place. Nonlinear stability analysis by Lin et al.[4] show convincingly that such profiles are obtained in a model that includes elastic effects, thus emphasizing the importance of elasticity in a system containing the dynamic contact line for the first time. There are many investigations of instability at the dynamic contact lines;[4,28,29] however, they contain gravity as an important force. Whereas greater generalization is achieved, drop sizes and thin-film thicknesses considered here are sufficiently small that gravity is negligible.

The present work concentrates on the elastic effects. A model for the dynamics of wetting in the form of α as a function of U (or $\frac{dr_o}{dt}$) for nematic liquid crystals is not available and is considered below. The equations governing momentum balances for the flow field must be solved along with the equations governing the orientation of the director vector, where the momentum and orientation are coupled. One key feature in the fluid mechanics of a dynamic contact line is that the shear stress becomes infinite at the contact line. de Gennes[30] circumvented this problem by using a cutoff at the molecular scale to isolate the region of singularity, which is also used below. A cutoff at local film thickness h^* implies that the films of thicknesses less than h^* as we go forward to the contact line are ignored in the analysis. The actual contact line is assumed to be at a distance comparable to h^* from the region of thickness h^*.

The equations of motion for the case of a plate plunged into the pool of liquid, that is, forced spreading, are obtained using standard approximations. This results in α as a function of substrate speed U, a result that is sought. It has been used to explain the spreading kinetics of a drop, spontaneous spreading, which is how many experiments are conducted.

II. METHODS

II.I. Formulation. Consider Figure 1b where a plate is plunged into a liquid. Rectangular coordinates, with the origin at the dynamic contact line are shown, with x in the tangential direction and y in the normal direction with respect to the surface of the plate. The dynamic contact angle α is assumed to be small. As a result, the slopes of profiles are small everywhere and, far from the contact line, the profile is given by $h \sim \alpha \cdot x$ where $\tan \alpha \approx \alpha$. It is interesting that when the results of the approximation are compared to experiments, good comparisons are seen even up to $\alpha = 90°$.[31,32] Consequently, this approximation is not considered very confining, as no result contrary to those seen in the experiments isand the effects of gra observed. Further, at the contact line, $\frac{dh}{dx} = \lambda$, and this angle usually cannot be observed under the magnification shown in Figure 1. The macroscopic length scale L satisfies $\rho g L^2/\gamma \ll 1$, and the effects of gravity are neglected. Specifically, if in Figure 1b, the magnitude of the film thickness is H, the length scale in the tangential direction is L, and the velocities are scaled with U, then for $H \ll L$, the continuity equation leads to a negligible value of v_y and it is observed that v_x does not vary in the x-direction. This makes v_x independent of x. These items constitute the lubrication theory approximation.[33] The equations of motion are at quasistatic condition $\mathbf{0} = -\nabla(p + \Phi) + \nabla \cdot \boldsymbol{\tau}$ where $\boldsymbol{\tau}$ is the Leslie–Ericksen stress tensor[16] for the anisotropic fluid

$$\tau_{ji} = \mu_1 n_k n_m d_{km} n_i n_j + \mu_2 n_j N_i + \mu_3 n_i N_j + \mu_4 d_{ji} + \mu_5 n_j n_k d_{ki} + \mu_6 n_i n_k d_{kj}$$

and the rate of deformation tensor, angular momentum of a director, and vorticity tensor are, respectively, $2d_{ij} = v_{i,j} + v_{j,i}$, $N_i = -\omega_{ik} n_{k,j}$, and $2\omega = v_{i,j} - v_{j,i}$. The potential Φ is given by eq 2. Once v_y is neglected and all variations in the x-direction are neglected, except on pressure, the equations of motion are greatly simplified for flow between two parallel plates, and these are taken from Chandrasekhar[16] below. The equation of motion in the y- direction is given by $\frac{\partial}{\partial y}(p + \Phi) = 0$. Here, $(p + \Phi)$ is dependent only on x and leads to $a = \frac{d}{dx}(p + \Phi)$ independent of y. Here, Φ is the Oseen–Frank–Zochner potential,[16] which Chandrasekhar had ignored in the presence of a large shear. The momentum balance in the x-direction after one integration over y leads to

$$g(\theta)\frac{dv_x}{dy} = ay + c \tag{3}$$

The conservation of angular momentum is given by

https://doi.org/10.1021/acs.jpcb.2c08552
J. Phys. Chem. B 2023, 127, 3071−3078

$$2f\frac{d^2\theta}{dy^2} + \frac{df}{d\theta}\left(\frac{d\theta}{dy}\right)^2 + (ay + c)\frac{\lambda_1 + \lambda_2 \cos 2\theta}{g(\theta)} = 0 \quad (4)$$

where

$$f(\theta) = k_{11}\cos^2\theta + k_{33}\sin^2\theta \quad (5)$$

$$g(\theta) = \frac{1}{2}[2\mu_1 \sin^2\theta \cos^2\theta + (\mu_5 - \mu_2)\sin^2\theta + (\mu_6 + \mu_3)\cos^2\theta + \mu_4] \quad (6)$$

The angle θ is the angle between director $\mathbf{n}$ and the x axis; see Figure 1b. In addition, $\lambda_1 = \mu_2 - \mu_3$ and $\lambda_2 = \mu_5 - \mu_6$. All μ_i are viscosities. These viscosities describe the anisotropic behavior of the liquid and, as the temperature is increased above the nematic to isotropic transition temperature, the fluid becomes Newtonian and needs only one viscosity, which defines the stress tensor as being proportional to the rate of deformation tensor. This proportionality constant is μ_4. Consequently, it is possible to suggest that, as the transition temperature is crossed from below, all viscosities become zero except for μ_4. The coefficients k_{11} and k_{33} are splay and bend moduli, respectively, as noted after eq 2. The boundary conditions for the fluid flow are zero shear, $dv_x/dy = 0$, at $y = h$ and $v_x = U$ at $y = 0$. The condition of anchoring at the nematic liquid crystal−air interface varies, but the condition $\theta = \pi/2$ (director is perpendicular to the interface in Figure 1b) at $y = h$ is often encountered.[34] The other anchoring at $y = 0$ is treated here as $\theta = \theta_o$ at $y = 0$. For simplicity, θ_o is assumed to be zero below, that is, parallel to the solid surface. It is assumed that $k_{11} = k_{33} = k$ and all viscosities are set to zero except for μ_4, which is denoted μ. Both of these are common assumptions,[18] and so the fluid is being modeled effectively as a Newtonian fluid with isotropic elasticity. The importance of elasticity at the moving contact line is made apparent in the work of Lin et al.[4] Another condition, that of zero flow rate into the wedge, is also used.

As noted earlier, the fluid mechanics involving contact lines show infinite stresses there. Following de Gennes,[30] a cutoff is that which isolates a tiny segment containing the singularity. L is a representative macrolength scale for the problem, and ε is the dimensionless cutoff, which is very small in magnitude. The contact line is placed at $x \sim O(\varepsilon L)$ where h (or h^* from before) $= \varepsilon L$.

II.II. Solution. The solutions to eqs 3−6 with the approximations given earlier, are

$$\theta = \theta_o + \left(\frac{\pi}{2} - \theta_o\right)\frac{y}{h} \quad (7)$$

$$\frac{d}{dx}(p + \Phi) = \frac{3\mu U}{h^2} \quad (8)$$

and

$$v_x = U + \frac{3U}{h^2}\left(\frac{y^2}{2} - hy\right) \quad (9)$$

Both sides of eq 8 are functions of x only. Note the singularity in the pressure gradient is due to viscous stresses at the contact line $h = 0$. Since $p + \Phi$ is independent of y, the Laplace pressure, which is the product of surface tension and curvature, can be calculated at the surface as shown below. The expression for curvature can be simplified under the assumption that $\left(\frac{dh}{dx}\right)^2 \ll 1$, which is appropriate using lubrication theory. Using those assumptions, the potential also simplifies and one obtains

$$p + \Phi = -\gamma\frac{d^2h}{dx^2} + k\theta_y^2 \quad (10)$$

where from eq 7, $\theta_y^2 = \frac{((\pi/2) - \theta)^2}{h^2}$, which provides the second singularity under strong anchoring. In principle, all quantities which vary in the x-direction, such as the Laplace pressure, can be neglected. However, the latter provides the only resistive force in forced spreading and the only driving force in spontaneous spreading and is retained. Consequently, all other terms that occur below are of the order of this small term. eq 10 and the above expression for θ_y^2 can be combined to yield an equation for the shape of the profile

$$\frac{d}{dx}\left[-\gamma\frac{d^2h}{dx^2} + k\frac{((\pi/2) - \theta_o)^2}{h^2}\right] = \frac{3\mu U}{h^2} \quad (11)$$

It is intended below to obtain an asymptotic solution by using successive approximation starting with $h \sim \alpha x$ and $\frac{dh}{dx} \sim \alpha$, a profile that holds far from the contact line. Thus, iteratively $h \sim \alpha x$ is inserted in eq 11 on the right-hand side and the left hand is again used to recalculate h.[34−36] This will also be the outer solution in our forthcoming singular perturbation problem, which is

$$\frac{1}{2}\left[\alpha^2 - \left(\frac{d\hat{h}}{d\hat{x}}\right)^2\right] - \frac{k}{\gamma L}\frac{((\pi/2) - \theta_0)^2}{\hat{h}} = \frac{3\mu U}{2\gamma\alpha}\ln\frac{1}{\hat{x}} \quad (12)$$

where $\hat{h} = h/L$ and $\hat{x} = x/L$. The inner solution is $\frac{d\overline{h}}{d\overline{x}} \sim \lambda$ where $\overline{h} = \hat{h}/\varepsilon$ and $\overline{x} = \hat{x}/\varepsilon$. It describes the profile in the immediate vicinity of the contact line. The slopes are matched by forcing $\hat{x}$ to go to ε from below and getting $\overline{x}$ to go to infinity, that is, extrapolating one solution into the domain of other. eq 13 is obtained.

$$\frac{1}{2}(\alpha^2 - \lambda^2) = \frac{k}{\varepsilon\gamma L}\left(\frac{\pi}{2} - \theta_o\right)^2 + \frac{3\mu U}{2\alpha\gamma}\ln\left|\frac{1}{\varepsilon}\right| \quad (13)$$

Matching also requires that $\frac{k}{\varepsilon\gamma L}$ and $\frac{\mu U}{\gamma}\ln\left|\frac{1}{\varepsilon}\right|$ be both $\sim O(1)$. Details of the various steps in above are given in the Supporting Information.

III. RESULTS AND DISCUSSION

Returning to eq 13, if $k = 0$, then the Brochard-Wyart and de Gennes[37] correction for the wetting kinetics of Newtonian nonwetting liquids, given by Voinov−Hoffmann−Tanner's rule,[38] is obtained. Note that the result is in the form of $\frac{dr_o}{dt} \propto \alpha(\alpha^2 - \lambda^2)$, somewhat different from the results of Neogi and Miller[7] given earlier, but not by much. In the term containing elasticity in eq 13, both ε in the denominator and k in the numerator are small. If this ratio is large compared to the second term on the right, then the drop will be frozen at an angle other than λ; this will be an elastic drop. The term $\frac{k}{\gamma L}$, which is the ratio between elasticity and surface tension, could be large when $L \sim V^{1/3}$ and the drop volume V is very small. For a spreading drop, an effort is made to keep the drop size

https://doi.org/10.1021/acs.jpcb.2c08552
J. Phys. Chem. B 2023, 127, 3071−3078

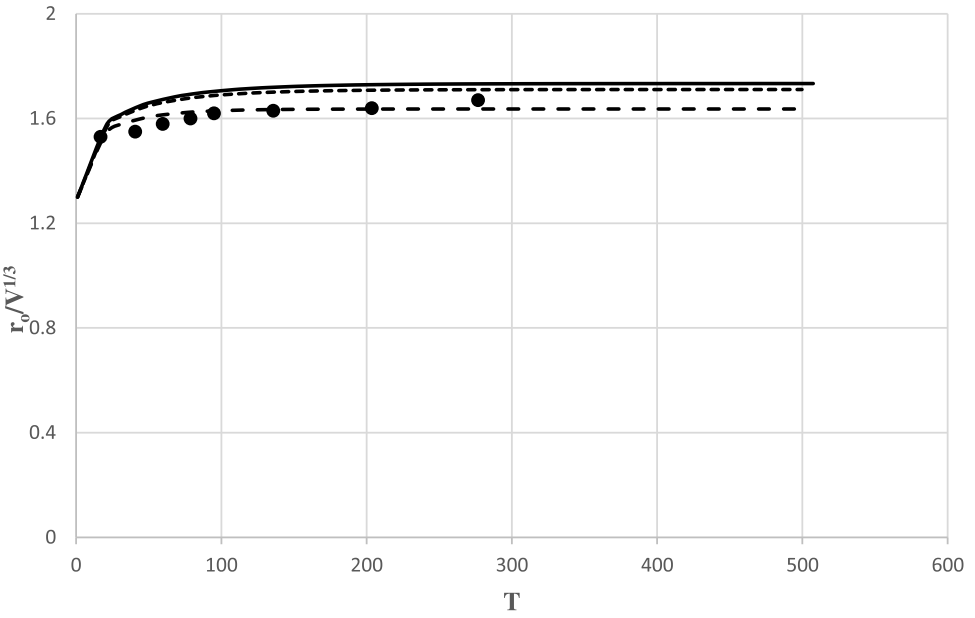

Figure 2. Wetting kinetics of a drop for $\lambda = 14°$ and $\frac{k}{\varepsilon\gamma V^{1/3}}$ of 0 (bold), 10^{-3} (dotted), and 5×10^{-2} (dashed), with $T = \frac{\gamma}{\mu V^{1/3}}\left[\ln\left|\frac{1}{\varepsilon}\right|\right]^{-1} \cdot t$. Data from Lin et al.[15] for one case in black dots have been plotted and fall on the dashed curve.

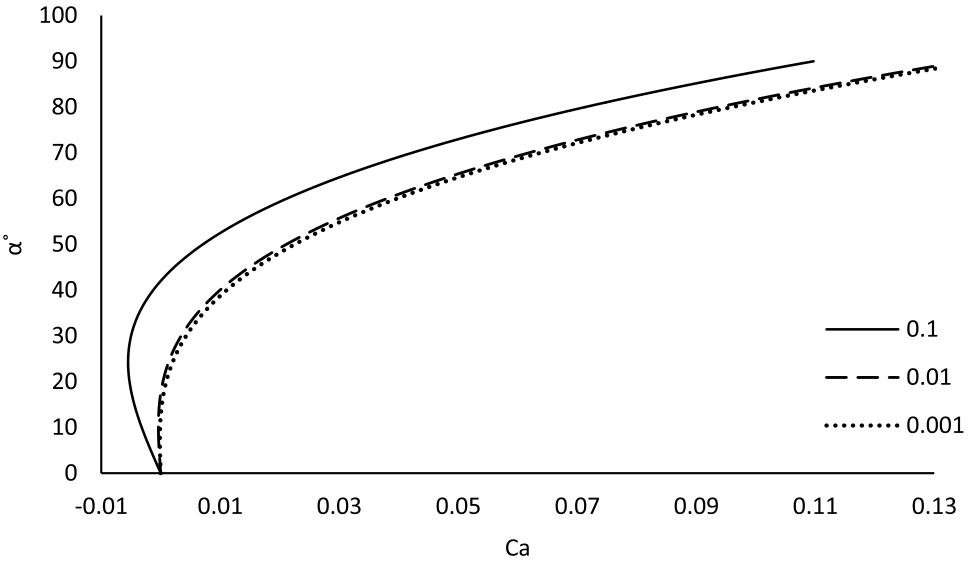

Figure 3. Equation 13 has been plotted for $\varepsilon = 10^{-4}$, for $\lambda = 12°$ and $\frac{k}{\varepsilon\gamma L} = 0.1$, 0.01, and 0.001 successively from top to bottom. The case where the elastic effect is large shows two values of α, one at 42°, and the other at one at 12°, both when $Ca = 0$. Others appear to show 12° at $Ca = 0$. For the case of elasticity of 0.1, Ca is approximately zero at $\alpha = 42°$ and remains zero till $\alpha = 0°$.

small so that gravity is negligible and does not affect the drop shape, which then will have a segment of the sphere profile.

It has been observed by Poulard and Cazabat[13] that some drops did not move, and they attributed this behavior to low humidity and the effect of low humidity on the solid substrate. They follow the effects of drop sizes less closely, but note that some drops had volumes less that $10^{-2}\mu$l. The small drop would not move if the group $\frac{k}{\varepsilon\gamma L}$ is large with $L \sim V^{1/3}$. More details on numerical estimates are given below.

In addition to the above dimensionless group, there is also the capillary number $Ca = \frac{\mu U}{\gamma}$, which is the ratio between viscous and surface tension forces. If the elastic group is divided by the capillary number, one has the more conventional inverse Erikson number, $\hat{E} = \frac{k}{\mu UL} = \frac{k}{\gamma L}/\frac{\mu U}{\gamma}$, which is the ratio of elastic to viscous forces.

III.I. Small Drops. To apply lubrication theory approximation to axisymmetric drops, it is necessary to require the drops to be thin and flat. This implies that the basal radius r_o is large and the curvature along the basal circle can be ignored and eq 13 will apply. To convert eq 13 into the equation for a spreading drop, we divide both the numerator and denominator in $\frac{dr_o}{dt}$ by $V^{1/3}$. Small drops have a segment of sphere profiles and $\alpha \approx 4V/(\pi r_o^3)$. The dependent variable is written in terms of $r_o/V^{1/3}$ and, on integration with no

https://doi.org/10.1021/acs.jpcb.2c08552
J. Phys. Chem. B 2023, 127, 3071−3078

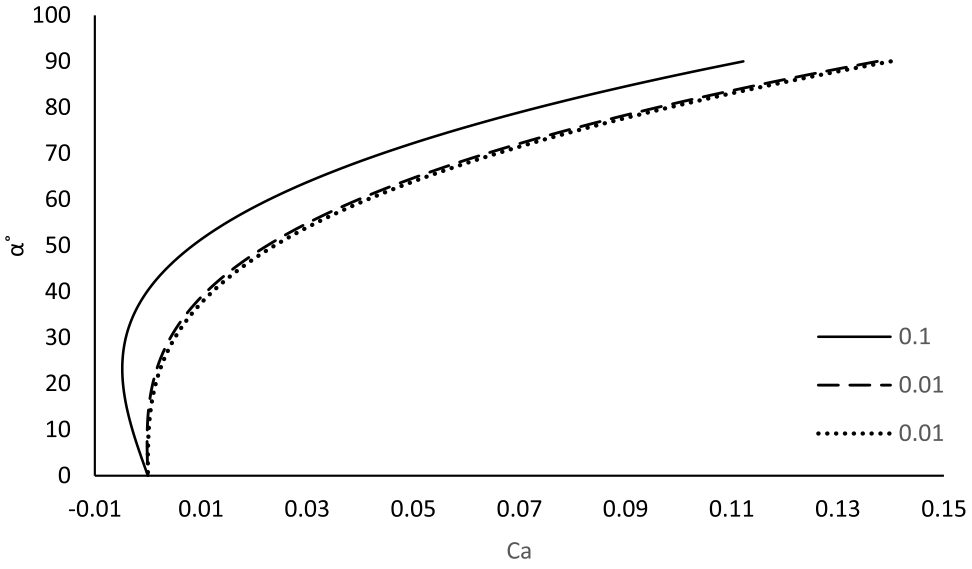

Figure 4. Equation 13 has been plotted for $\varepsilon = 10^{-4}$, for $\lambda = 0°$ and $\frac{k}{\varepsilon\gamma L} = 0.1$, 0.01, and 0.001 successively from top to bottom. The case where the elastic effect is large shows two values of α, one at 41°, and the other at nearly zero, both at $Ca = 0$. Others appear to show zero at $Ca = 0$.

elasticity, one obtains $r_o/V^{1/3}$ as a function of $t_o/V^{1/3}$ noted earlier. However, in the case of nematic liquid crystals, one extra $V^{1/3}$ will remain from the first term on the right-hand side in eq 13. The results of numerical integration are shown in Figure 2 for $\lambda = 14°$ to compare with the experiments of Lin et al.[15] The estimate for the initial value of $r_o/V^{1/3} = 1.3$ was obtained as a part of the fitting process. The comparison provides estimates for $\frac{k}{\varepsilon\gamma V^{1/3}} \sim 5 \times 10^{-3}$ and $\frac{\gamma}{\mu}\left[\ln\left|\frac{1}{\varepsilon}\right|\right]^{-1}$ of 10^{-3}. More iterations would have given a better fit, but the data suffer a little additional scatter that occurs when we have to read off the numbers from the graph. So the parameter estimation was left at the primary estimate. Only one set of data were analyzed as all data sets fall in the narrow range of $r_o/V^{1/3} = 1.5$ to 1.7. The set that was picked had the lowest starting value of $r_o/V^{1/3}$.

At the value of $\frac{k}{\varepsilon\gamma V^{1/3}} = 5 \times 10^{-2}$, the plot for $r_o/V^{1/3}$ is almost flat and shows a very shallow maximum followed by equilibration. The maximum can only be observed when plotted on a more expanded scale than in Figure 2. This is recoil, where the advancing contact line stops advancing and then recedes. At the value of $\frac{k}{\varepsilon\gamma V^{1/3}} = 0.1$, the contact line only recedes. Neither of these two last cases has been shown in Figure 2.

Lin et al.[15] make a point that their data show that the spreading rates decrease with decreasing drop volumes. As V decreases, $\frac{k}{\varepsilon\gamma V^{1/3}}$ increases, and as Figure 2 shows, the spreading rates slow down. In fact, it has been observed earlier in eq 13 that if L or $V^{1/3}$ is very small, the drop may not be seen to spread.[13] The plots for $\lambda = 0°$ are similar and have been shown in the Supporting Information.

III.II. More on Including Receding Contact Lines. In Figure 3, α has been plotted against Ca, using eq 13, for cutoff thickness $\varepsilon = 10^{-4}$ and for $\lambda = 12°$, and in Figure 4, for $\lambda = 0°$. Different values of $\frac{k}{\varepsilon\gamma L}$ have been used. If molecular dimension is chosen for εL, then ε will be lower, but if a precursor thin film is also included in the cutoff, then ε will rise to 10^{-4} as chosen here. In Figure 3, when $\frac{k}{\varepsilon\gamma L}$ is 0.1, then there are two values of α at equilibrium ($U = 0$ or $Ca = 0$), one at 42° and one at 0°, which gives rise to a loop that passes into negative values of Ca. This appears to be an example of recoil mentioned earlier. The loops are absent at the lower values of $\frac{k}{\varepsilon\gamma L}$ where α reaches 12° (or very close) at $Ca = 0$ and falls precipitously to $\alpha = 0$ along the vertical line $Ca = 0$. Thus, for the highest

elasticity, the drop starts spreading at large α with the largest velocity (or Ca). This velocity slows down smoothly to 42° where $Ca = 0$, that is, at equilibrium. Thereafter, Ca turns negative, which implies that the contact line is receding, until it reaches equilibrium at 12°. For lower elasticities, the contact angle drops from 12 and 0° is through $Ca = 0$, and the drop is frozen at the position reached by the contact line when 12° is attained.

Figure 4 deals with the case in which $\lambda = 0°$. At the largest value of $\frac{k}{\varepsilon\gamma L}$, the plot describes a loop before reaching $\alpha = 0°$. There are no loops for smaller values of $\frac{k}{\varepsilon\gamma L}$ and plots reach $\alpha = 0°$. The fact that two values of the dynamic contact angle exist for some capillary numbers can be used to explain recoil: if a drop is allowed to spread spontaneously, then it spreads rapidly at first (high contact angle) and then slows down (lower contact angle). Then it can reverse direction and recede, but still lowering the contact angle. This recoil has been noted by Lin et al.[15] for one case of EBBA that progressed too fast for the investigators to quantify. In general, what can be observed seems to depend on viscosity. As an aside, smectic liquid crystals (water-oil-surfactant) were so viscous that drops dried out in an environment controlled to prevent evaporation, with no observable spreading. Figure 4 differs from Figure 3 only by a small change in the new equilibrium contact angle from 42 to 41°, a point to which we return later.

These loops are also observed in Newtonian (or inelastic) liquids, in a region where $Ca < 0$ (as in this work) but for α between λ and zero (unlike in this work where α lies between

https://doi.org/10.1021/acs.jpcb.2c08552
J. Phys. Chem. B 2023, 127, 3071−3078

some value $\alpha_e > \lambda$, and zero). For a Newtonian fluid, this condition is in the range of receding contact angles. de Gennes[39] suggested that, as the plate is dragged out with increasing velocities, the tip of the loop is reached beyond which there is no solution. The entrainment of a thin film then takes place, leading to what is well known as the process of dip coating. This feature has been verified experimentally for Newtonian fluids.[40,41] This is an example of forced spreading, and there are no experimental observations with nematic liquid crystals for receding contact lines. For completion, we note that the nose of the loop is located at

$$Ca \times \ln\left|\frac{1}{\varepsilon}\right| = \alpha^{*3} \tag{14}$$

$$\frac{1}{2}[\alpha^{*2} + \lambda^2] = \frac{k}{\varepsilon\gamma L}\left(\frac{\pi}{2} - \theta_e\right)^2 \tag{15}$$

where the stars denote the conditions at the tip of the nose. By setting $U = 0$ in eq 13, one equilibrium is obtained at

$$\alpha_e = \sqrt{\lambda^2 + \frac{k}{\varepsilon\gamma L}(\pi - \theta_e)^2} \tag{16}$$

The other equilibrium ($U = 0$) in eq 13 is $\alpha_e = 0$. In case λ is small, α_e will be determined by the elastic effects. Hence, α_e in Figures 3 and 4 are calculated to be 42 and 41° for the cases of large elasticity and low or zero λ.

III.III. Parameter Estimates. As mentioned earlier, ε was originally suggested to be of the molecular dimension,[29] but later work by de Gennes[42] suggests that it can equal the thin-film thickness of the precursor, in which case, it will be much larger and ε for this case has been taken to be 10^{-4}. Values calculated from other experiments[41] are much smaller. We can take $\varepsilon = 10^{-6}$ as a lower value. If $\frac{k}{\varepsilon\gamma L} = 0.1$, the large value in our case, then with $k = 5 \times 10^{-7}$ dynes, $\gamma = 25$ dynes/cm, we calculate $V = 6\ \mu$l, but for $\varepsilon = 10^{-4}$, $L \sim V^{1/3}$ is calculated to be 0.002 cm and V is found to be $8 \times 10^{-6}\ \mu$l, which values are very low and cannot be reached experimentally. However, if $\varepsilon = 10^{-6}$ then, in the last case, one has $L = 0.2$ cm, $V = 2\ \mu$l, both of which are very reasonable values. Similarly, when $\frac{k}{\varepsilon\gamma L} = 0.1$, then, for $\varepsilon = 10^{-6}$, L is found to be 0.2 cm, and, for $\frac{k}{\varepsilon\gamma L} = 0.001$ and $\varepsilon = 10^{-4}$, L is found to be 0.2 cm. That is, the drop volumes can often be chosen in experiments to be in a reasonable range. As plotted, Figures 3 and 4 do not change much if ε is changed 10^{-4} to 10^{-6} because the only change that occurs is in the logarithmic term in eq 13, which is relatively insensitive to the values of ε.

It is interesting that de Gennes'[30] suggests that one can equate surface work to viscous dissipation to get the dynamic contact angle that does not quite manage to bring in the elastic effect. The reason is that the elastic effect does not contribute directly to the viscous dissipation, except indirectly by changing the local film thickness.

IV. CONCLUSIONS

Elasticity plays a major role in the wetting kinetics of a nematic liquid crystal. It leads to an extra volume dependence in the relation connecting the dynamic contact angle to the spreading rate. It also brings about a second equilibrium. A recoil mechanism may arise to relieve the pressure generated by the elastic stresses. The continuum theory of nematic liquid crystals is sufficient to explain the above observations. However, the theory in which the wetting kinetics is determined by equating the viscous dissipation in a wedge to the surface work done does not work because the normal stresses do not lead to viscous dissipation, although the theory has been very successful otherwise. The alternate theory presented here is force based.

■ ASSOCIATED CONTENT

Supporting Information

The Supporting Information is available free of charge at https://pubs.acs.org/doi/10.1021/acs.jpcb.2c08552.

Molecular model; mathematical development and responses (PDF)

■ AUTHOR INFORMATION

Corresponding Author

P. Neogi − *Chemical and Biochemical Engineering, Missouri University of Science and Technology, Rolla, Missouri 65409-1230, United States;* orcid.org/0000-0003-4618-7029; Email: neogi@mst.edu

Authors

Xianjie Qiu − *Chemical and Biochemical Engineering, Missouri University of Science and Technology, Rolla, Missouri 65409-1230, United States;* Present Address: Guangzhou Regenerative Medicine and Health, Guangzhou Laboratory, Guangdong Laboratory, Guangzhou, PRC

Amer Al-Shareef − *Chemical and Biochemical Engineering, Missouri University of Science and Technology, Rolla, Missouri 65409-1230, United States;* Present Address: Chemical and Petroleum Engineering, Faculty of Engineering, Elmergib University, Khoms, Libya

Complete contact information is available at: https://pubs.acs.org/10.1021/acs.jpcb.2c08552

Notes

The authors declare no competing financial interest.

■ ACKNOWLEDGMENTS

The authors thank Professor Louis Biolsi for proofing and making editorial suggestions. Missouri University of Science and Technology funded the research.

■ REFERENCES

(1) Miller, C. A.; Neogi, P. *Interfacial Phenomena, Equilibrium and Dynamic Effects*, 2nd ed.; CRC Press, Taylor and Fracis: Boca Raton, 2008; p 61.

(2) Tsuji, T.; Rey, A. D. Effect of long range order on sheared liquid crystalline materials. Part 1: compatibility between tumbling behavior and fixed anchoring. *J. Non-Newtonian Fluid Mech.* **1997**, *73*, 73127−73152; Effect of long range order on sheared liquid crystalline materials: Flow regimes, transition, and rheological phase diagrams. *Phys. Rev. E* **2000**, *62*, 8141−8151.

(3) Rey, A. D.; Denn, M. M. Dynamical phenomena in liquid crystalline materials. *Ann. Rev. Fluid Mech.* **2002**, *34*, 233−266.

(4) Lin, T.-S.; Kondic, L.; Thiele, U.; Cummings, L. J. Modelling spreading dynamics of nematic liquid crystals in three spatial dimensions. *J. Fluid Mech.* **2013**, *729*, 214−230.

(5) Chen, R. H. *Liquid Crystal Displays: Fundamental Physics and Technology*; Wiley: New York, 2011.

(6) Gupta, V. K.; Skaife, J. J.; Dubrovsky, T. B.; Abbott, N. B. Optical amplification of ligand receptor binding using liquid crystals. *Science* **1998**, *279*, 2077−2080.
(7) Neogi, P.; Miller, C. A. Spreading kinetics of a drop on a smooth solid surface. *J. Colloid Interface Sci.* **1982**, *86*, 525−538.
(8) Cox, R. G. The dynamics of spreading of liquids on a solid surface. Part 1. Viscous flow. *J. Fluid Mech.* **1986**, *168*, 169−194.
(9) Bascom, W. D.; Cottington, R. L.; Singleterry, C. L. Dynamic Surface Phenomena in the Spontaneous Spreading of Oils on Solids. In *Contact Angle, Wettability and Adhesion*; Gould, R. F., Ed.; ACS Publications: Washington, D.C., 1964; pp 355−380.
(10) Williams, R. The advancing front of a spreading liquid. *Nature* **1977**, *266*, 153−154.
(11) Neogi, P. Contact line instability in spontaneous spreading of a drop on a solid surface. *J. Fluid Mech.* **2001**, *428*, 171−183.
(12) Cousins, J. R.; Duffy, B. R.; Wilson, S. K.; Mottram, N. J. Young and Young-Laplace equations for a static ridge of nematic liquid crystals, and transition between equilibrium states. *Proc. R. Soc. A* **2022**, No. 20210849.
(13) Poulard, C.; Cazabat, A.-M. Spontaneous spreading of nematic liquid crystals. *Langmuir* **2005**, *21*, 6270−6276.
(14) Parry, E.; Kim, D.-J.; Castrejon-Pita, A. A.; Elston, S. J.; Morris, S. M. Formation of radially aligned and uniform nematic liquid crystal droplets via drop on demand inkjet printing into a partially wet polymer layer. *Opt. Mat.* **2018**, *80*, 71−76.
(15) Lin, C.-M.; Neogi, P.; Ybarra, R. M. Statics and dynamics of contact lines of nematic liquid crystals on mica. *Chem. Eng. Sci.* **2000**, *55*, 37−42.
(16) Chandrasekhar, S. *Liquid Crystals*, 2nd ed.; Cambridge University Press: Cambridge, 1992.
(17) Gruler, H. The elastic constants of a nematic liquid crystal. *Z. Naturforsch., A* **1975**, *30*, 230−234.
(18) de Gennes, P-G.; Prost, J. *The Physics of Liquid Crystals*, 2nd ed.; Oxford University Press: Oxford, 1993.
(19) Perez, E.; Proust, J. E.; Minassian-Saraga, T. Thin Liquid Films from Liquid Crystals. In *Thin Liquid Films*; Ivanov, I. B., Ed.; Marcel Dekker: New York, 1988; p 891.
(20) Neogi, P.; Zhang, X. Wettability of nematic liquid crystals. *J. Colloid Interface Sci.* **2001**, *237*, 145−146.
(21) Churaev, N. V. Contact angles and surface forces. *Colloid J.* **1994**, *56*, 631−636.
(22) Shmeliova, D. V.; Pasechnik, S. Y.; Kharalamov, S. S.; Zakharov, A. V.; Pozhidaev, E. P.; Barbashov, V. A.; Tkachenko, T. P. Capillary flows of nematic liquid crystal. *Crystals* **2008**, *26*, No. 1029.
(23) Patrício, P.; Silvestre, N. M.; Pham, C.-T.; Romero-Enrique, J. M. Filling and wetting transitions of nematic liquid crystals on sinusoidal substrates. *Phys. Rev. E* **2011**, *84*, No. 021701.
(24) Brown, C. V.; Bhadwal, A. S.; Edwards, A. M. J.; Sage, I. C.; Saxena, A.; Mottram, M. J. Frequency-controlled dielectricophroresis-driven wetting of nematic liquid crystals. *J. Phys. D: Appl. Phys.* **2022**, *55*, No. 285302.
(25) Mena, E.; Kondic, L.; Cummings, L. J. Dielectrowetting of a thin nematic liquid crystal layer. *Phys. Rev. E.* **2021**, *103*, No. 032702.
(26) Wei, H.-H.; Li, Y.-C. Conformal transitions of single polymer adsorption in poor solvent: Wetting transition due to molecular confinement induced line tension. *Phys. Rev. E* **2016**, *94*, No. 012501.
(27) Jérôme, B.; Biox, M. Wetting instability in nematic liquid crystals. *Europhys. Lett.* **1992**, *17*, 169−174.
(28) Lam, M. A.; Cummings, L. J.; Lin, T.-S.; Kondic, L. Three-dimensional coating flow of nematic liquid crystal on an inclined substrate. *Eur. J. Appl. Math.* **2015**, *26*, 647−669.
(29) Kondic, L.; Cummings, L. J. Instabilities of nematic liquid crystals. *Curr. Adv. Colloid Interface Sci.* **2021**, *55*, No. 101478.
(30) de Gennes, P.-G. The dynamics of spreading droplet. *C. R. Acad. Sci., Ser. II* **1984**, *298*, 111−115.
(31) Lopez, J.; Miller, C. A.; Ruckenstein, E. Spreading kinetics of liquid drops on solids. *J. Colloid Interface Sci.* **1976**, *56*, 460−468.
(32) Wang, X. D.; Lee, D. J.; Peng, X. F.; Lai, J. Y. Spreading dynamics and dynamic contact angle of non-Newtonian fluids. *Langmuir* **2007**, *23*, 8042−8047.
(33) Batchelor, G. K. *An Introduction to Fluid Dynamics*; Cambridge University Press: Cambridge, 1967; p 219.
(34) Faetti, S. Anchoring at the interface between a nematic liquid crystal and an isotropic substrate. *Mol. Cryst. Liq. Cryst.* **1980**, *23*, 217−231.
(35) Coddington, E. A. *An Introduction to Ordinary Differential Equations*; Prentice-Hall: Englewood Cliffs, N.J., 1968; p 201.
(36) Coddington, E. A.; Levinson, N. *The Theory of Ordinary Differential Equations*; McGraw-Hill: N.Y, 1955.
(37) Brochard-Wyart, F.; de Gennes, P.-G. Dynamics of partial wetting. *Adv. Colloid Interface Sci.* **1992**, *39*, 1−11.
(38) Kistler, S. Hydrodynamics of Wetting. In *Wettability*; Berg, J. C., Ed.; Marcel Dekker: N.Y, 1993; pp 311−431.
(39) de Gennes, P.-G. Deposition of Langmuir-Blodgett layers. *Colloid Polym. Sci.* **1986**, *264*, 463−465.
(40) Quéré, D. On the minimal velocity of forced spreading in partial wetting. *C. R. Acad. Sci., Ser. II* **1991**, *313*, 313−318.
(41) Al-Shareef, A.; Neogi, P.; Bai, B. Force based dynamic contact angles and wetting kinetics on a Wilhelmy plate. *Chem. Eng. Sci.* **2013**, *99*, 113−117.
(42) de Gennes, P.-G. Wetting: statics and dynamics. *Rev. Mod. Phys.* **1985**, *57*, 827−863.

https://doi.org/10.1021/acs.jpcb.2c08552
J. Phys. Chem. B 2023, 127, 3071−3078